PAPER

CrossMark
click for updates

Highly crystalline vanadium phosphate catalysts synthesized using poly(acrylic acid-co-maleic acid) as a structure directing agent

Mosaed Alhumaimess,† Zhongjie Lin, Nicholas F. Dummer, Stuart H. Taylor, Graham J. Hutchings and Jonathan K. Bartley*

Vanadium phosphate catalysts have been widely studied for the selective oxidation of alkanes to a variety of products, including maleic and phthalic anhydride. More recently they are starting to find use as low temperature liquid phase oxidation catalysts. For all these applications the synthesis of the precursor is key to the performance of the final catalyst. Changes in the preparation procedure can alter the morphology, surface area, crystallinity, oxidation state and the phases present in the final catalyst which can all affect the selectivity and/or activity of the catalyst. Adding a diblock copolymer, poly(acrylic acid-co-maleic acid) (PAAMA), during the synthesis was found to influence the crystallinity and morphology of the $VOHPO_4 \cdot 0.5H_2O$ precursors obtained. An optimal level of copolymer was found to form precursors that showed a faster, more efficient, activation to the active catalyst, whereas high amounts of copolymer formed thin platelets, which were prone to oxidise to undesirable V^{5+} phases under reaction conditions, reducing the selectivity to maleic anhydride.

1. Introduction

The synthesis of heterogeneous catalysts that contain the correct structural and textural properties is crucial. Although particle sizes can be controlled using a variety of methodologies, morphological control of particles has proved more difficult. The synthetic procedure for preparing oxide and phosphate catalysts is a key factor in controlling properties such as surface area, porosity and crystallinity, as well as the phases present in the final catalyst, all of which influence the catalyst performance. Previous studies have shown that relatively simple modifications to the preparation of vanadium phosphate materials, such as changing the solvent or reducing agent, can have a large effect on the final morphology, the chemical composition and hence, the catalyst performance.[1–18]

Templates are commonly used to control the structure of microporous and mesoporous materials, although they have not been so widely utilized for the synthesis of non-zeolitic classes of materials for which they can also be useful synthetic tools. Biomacromolecules, organic molecules that can act as nucleators, cooperative modifiers, matrixes or moulds are used by biological systems to aid morphological control. For example, sea shells, teeth and bones are all made from

the same materials but the fine control of nucleation and crystal growth results in unique structures.[19–21]

Diblock copolymers such as 2-poly(styrene-alt-maleic acid) (PSMA) and poly(acrylic acid-co-maleic acid) (PAAMA) have been used to try and mimic the effects of the biomacromolecules and have been shown to have a variety of different effects depending on the material synthesized. The morphology of PbS semiconductors has been shown to be dependant on the relative amounts of PSMA and cetyltrimethylammonium bromide (CTAB) added into the preparation mixture.[22] This is thought to be due to the copolymer preferentially interacting with particular crystal faces of the PbS leading to kinetic control over growth in the [111] and [100] directions. Using the PSMA–CTAB mixture star-like PbS particles with six symmetrical, perpendicular arms were formed, while cubic and spherical particles were produced when CTAB concentrations were increased.

Diblock copolymers have also been shown to promote the crystallization of particular phases, which Yu et al.[23] demonstrated could play a role in preventing urolithiasis. During the formation of CaO_x, the most common kidney stone composition, the addition of the PSMA was found to promote the growth of the tetragonal phase, which is easily expelled from the body, over the monoclinic phase that is difficult for the body to expel and hence, forms kidney stones. This effect was also shown to significantly improve the properties of mortar and concrete.[24] When PSMA was added into Portland cement it was found to promote the formation of anhydrous

Cardiff Catalysis Institute, School of Chemistry, Cardiff University, Main Building, Park Place, Cardiff, CF10 3AT, UK. E-mail: BartleyJK@cf.ac.uk
† Present address: Department of Chemistry, College of Science, Aljouf University, PO Box 2014, Sakaka, KSA.

calcium carboxylate over calcium hydroxide, which improves the strength of the material.[25]

For heterogeneous catalysts, increases in selectivity and/or activity can be obtained by preferentially exposing the active plane or preferentially forming the active phase. Previously, we demonstrated that a diblock copolymer, PSMA, could influence the crystallinity and morphology of a vanadium phosphate catalyst precursor.[26] In this study we have extended this work to investigate a more soluble copolymer, poly(acrylic acid-co-maleic acid) (PAAMA), which has allowed us to investigate different synthetic routes to the catalyst precursor and to study the effect of higher copolymer concentrations. This led to vanadium phosphate catalysts that show an improved performance for the selective oxidation of butane to maleic anhydride over those reported previously for the PSMA system.

2. Experimental

2.1. Catalyst preparation

The vanadyl hydrogen phosphate hemihydrate ($VOHPO_4 \cdot 0.5H_2O$) precursor was synthesised according to the literature[27] using two different methods denoted the VPO and VPD routes:

VPO route. V_2O_5 (2 g, Strem) and H_3PO_4 (1.66 ml, 85%, Aldrich) were added to isobutanol (2-methyl-1-propanol, 42.5 ml, Aldrich) and the mixture heated under reflux conditions for 16 h. The resultant pale blue solid was recovered by vacuum filtration, and washed with isobutanol (100 ml) and ethanol (100 ml), then dried in air at 110 °C. This material was denoted P-VPO0.

For the copolymer modified materials, V_2O_5 and H_3PO_4 were reacted in isobutanol with different amounts of PAAMA (poly (acrylic acid-co-maleic acid) solution. In a typical preparation, PAAMA (50%, average M_w = 3000, Aldrich) was added drop wise to a solution of H_3PO_4 (1.66 ml, 85%, Aldrich) and isobutanol (42.3 ml, anhydrous, Aldrich) in a round bottom flask. The solution was stirred at room temperature until a homogeneous solution formed. V_2O_5 (2 g, Aldrich) was then added under stirring, and the temperature raised to 110 °C and held at this temperature for 16 h. The resulting light blue solid was recovered by vacuum filtration, and washed with isobutanol (100 ml) and ethanol (100 ml), then dried in air at 110 °C. Three samples were prepared with different concentrations of PAAMA: 5 g L^{-1} (denoted P-VPO5), 15 g L^{-1} (denoted P-VPO15) and 25 g L^{-1} (denoted P-VPO25). The precursors P-VPO0, P-VPO5, P-VPO15 and P-VPO25 were activated at 400 °C *in situ* using a flow of 1.7% butane in air until steady state conversion and selectivity to maleic anhydride was observed, to give the respective catalysts, denoted C-VPO0, C-VPO5, C-VPO15 and C-VPO25.

VPD route. Vanadyl phosphate dihydrate ($VOPO_4 \cdot 2H_2O$) was synthesised by a standard method without any modification. In the typical preparation, V_2O_5 (10 g, Aldrich) and H_3PO_4 (45 ml, 85%, Aldrich) were heated under reflux conditions in water (120 ml) for 24 h. The resultant yellow $VOPO_4 \cdot 2H_2O$ solid was recovered by filtration, washed with water and acetone and dried in air (110 °C, 16 h).

$VOPO_4 \cdot 2H_2O$ (2 g) was then refluxed in isobutanol (40 ml) for 18 h. The resultant blue solid was recovered by hot filtration, washed with isobutanol (25 ml) and ethanol (33 ml) and dried in air (110 °C, 16 h). This material was denoted P-VPD0.

For the copolymer modified materials, the $VOPO_4 \cdot 2H_2O$ was refluxed in isobutanol with different amounts of PAAMA. In a typical preparation, PAAMA was added drop wise with stirring to isobutanol (40 ml, anhydrous, Aldrich) in a round bottom flask at room temperature until a homogeneous solution formed. $VOPO_4 \cdot 2H_2O$ (2 g) was added to this solution, which was stirred well and heated to the reflux temperature for 18 h. The pale blue solid was recovered by filtration and washed with isobutanol (25 ml) and ethanol (33 ml) and dried at 110 °C for 16 h. Three samples were prepared with different concentrations of PAAMA: 5 g L^{-1} (denoted P-VPD5), 15 g L^{-1} (denoted P-VPD15) and 25 g L^{-1} (denoted P-VPD25). The precursors P-VPD0, P-VPD5, P-VPD15 and P-VPD25 were activated at 400 °C *in situ* using a flow of 1.7% butane in air until steady state performance was observed, to give their respective catalysts, denoted C-VPD0, C-VPD5, C-VPD15 and C-VPD25.

2.3. Characterisation

Powder X-ray diffraction (XRD) was performed using a PANalytical X'Pert Pro fitted with an X'Celerator detector and a CuKα X-ray source operated at 40 kV and 40 mA. Scanning electron microscopy (SEM) analyses were carried out using a Carl Zeiss EVO-40 SEM equipped with a backscatter detector and an Oxford Instruments silicon lithium energy dispersive X-ray detector. The powder samples were sprinkled sparsely over carbon tape mounted on an aluminum stub before sputter coating with gold for *ca.* 5 min prior to the SEM analysis. Raman spectra were obtained using a Renishaw in *via* Raman Microscope fitted with a green Ar$^+$ laser (λ = 514.532 nm).

2.4. Catalyst testing

The oxidation of *n*-butane was carried out in a fixed bed microreactor with 0.2 g of catalyst. *n*-Butane and air were introduced into the reactor *via* calibrated mass flow controllers to give a feedstock composition of 1.7% *n*-butane in air. Catalyst precursor samples were activated *in situ* by heating the sample from room temperature to 400 °C at a rate of 3 °C min^{-1}. The reaction products were fed *via* heated lines to an on-line gas chromatograph for analysis. The reactor comprised a stainless steel tube with the catalyst held in place by plugs of quartz wool. A thermocouple was located in the centre of the catalyst bed and temperature control was typically better than ±1 °C. Carbon mass balances were typically 94–106%.

3. Results and discussion

3.1. Catalyst precursor characterisation

The VPO precursors (P-VPO0, P-VPO5, P-VPO15 and P-VPO25) were examined by XRD and the diffraction patterns were

observed to be typical of $VOHPO_4 \cdot 0.5H_2O$ (Fig. 1a). However, a change in morphology was observed as the concentration of PAAMA increased. In the standard precursor, P-VPO0, the (220) reflection was the most intense. The intensity of this

reflection decreased as the concentration of PAAMA added increased, while the (001) reflection increased with PAAMA addition. The different relative intensities of the (001) and (220) reflections have been shown to be characteristic of two
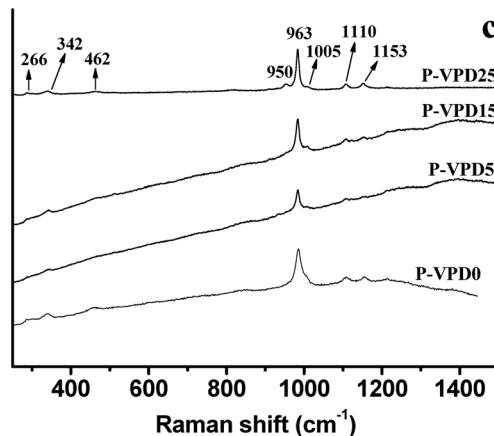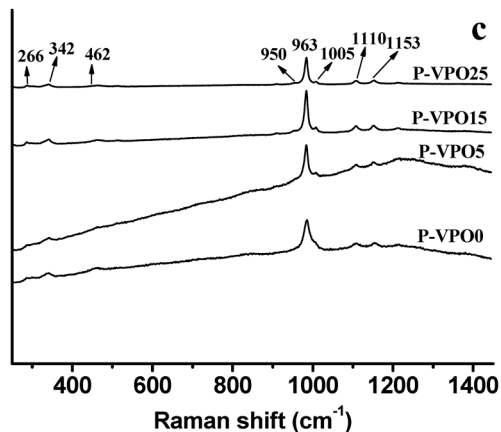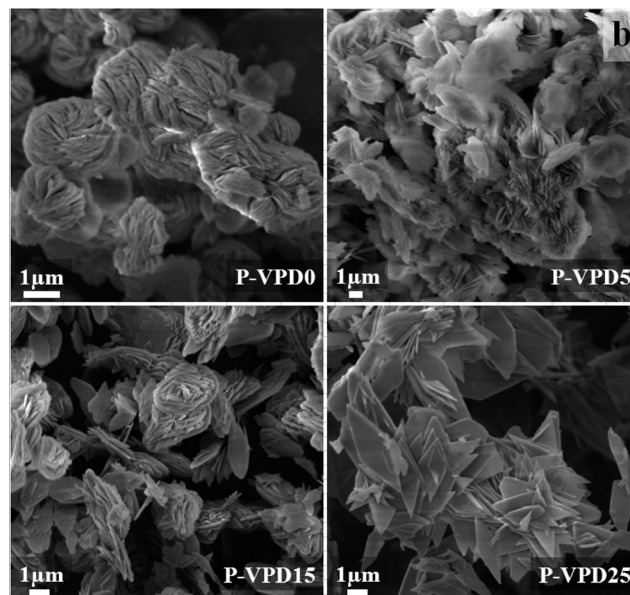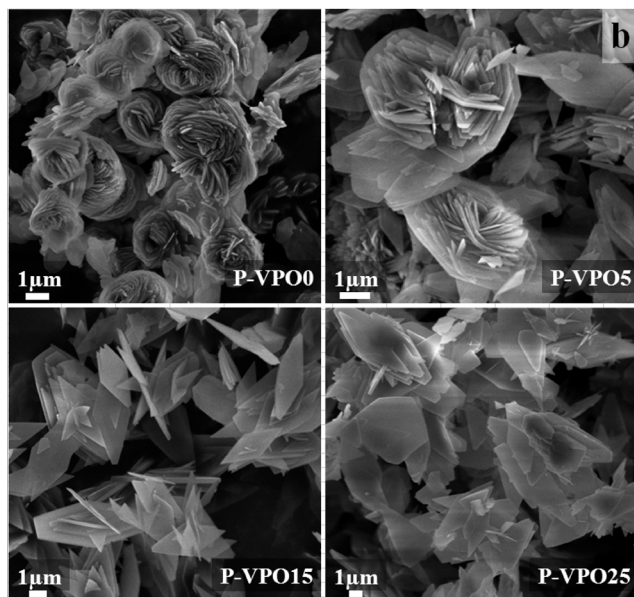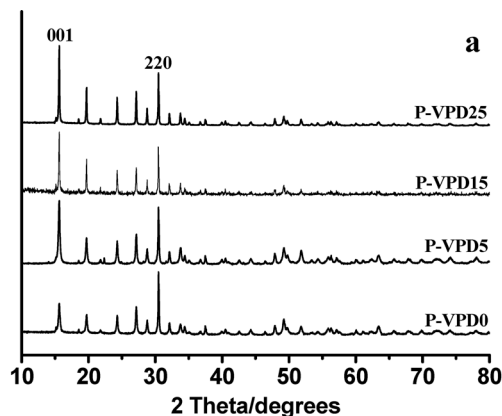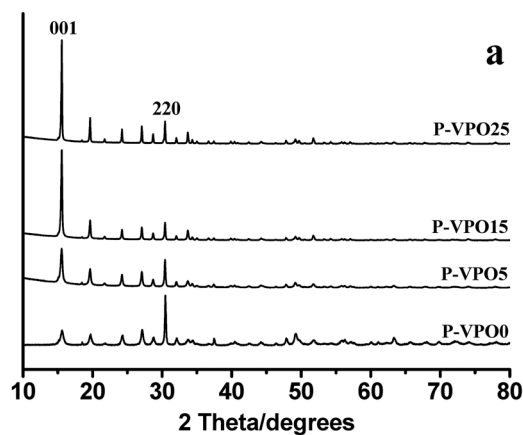

Fig. 1 (a) Powder XRD patterns, (b) SEM micrographs and (c) Raman spectra of P-VPO precursors.

Fig. 2 (a) Powder XRD patterns, (b) SEM micrographs and (c) Raman spectra of the P-VPD precursors.

distinct morphologies of $VOHPO_4 \cdot 0.5H_2O$.[15–18] The pattern with the (220) reflection as the dominant feature is typical of rosette-like structures, whereas the pattern with the (001) reflection as the dominant feature is typical of rhomboidal platelet structures. SEM analyses confirmed the morphology suggested by the XRD patterns (Fig. 1b). Generally, with higher concentrations of PAAMA in the preparation the number of rosette-like agglomerates decreased and the proportion of platelets increased. The standard precursor, P-VPO0 comprises rosette-like morphology, P-VPO5 comprises characteristic rosette-like agglomerates with isolated rhomboidal platelets, P-VPO15 comprises only isolated rhomboidal platelets and P-VPO25 comprises isolated rhomboidal and irregular platelets. This change in morphology can be attributed to the co-polymer behaving as a structure directing agent that prevents the growth of crystals in the direction of certain planes, and directs growth in particular directions. Raman spectroscopy was used to investigate whether there was any PAAMA present in the precursors (Fig. 1c). However, no PAAMA was detected and the spectra were typical of $VOHPO_4 \cdot 0.5H_2O$.

The PAAMA was observed to have a similar effect on the VPD precursors as the VPO materials. XRD confirmed that all precursor materials (P-VPD0, P-VPD5, P-VPD15 and P-VPD25) were $VOHPO_4 \cdot 0.5H_2O$ phase (Fig. 2a) and as for the VPO precursors, the addition of PAAMA decreased the (200) reflection and increased the (001) reflection, characteristic of a change in morphology from rosettes to platelets. SEM analyses of the precursors (Fig. 2b) confirmed the X-ray diffraction results. P-VPD0 comprised a rosette-like morphology, P-VPD5 comprised mainly of rosette agglomerates, P-VPD15 comprised rosette-like agglomerates with isolated rhomboidal platelets and P-VPD25 comprises isolated rhomboidal platelets. Again, Raman spectroscopy demonstrated that all precursors were typical of the $VOHPO_4 \cdot 0.5H_2O$ and there was no residual PAAMA detected (Fig. 2c).

It is apparent in this study that the addition of PAAMA to the precursors prepared *via* either the VPO or VPD route enhances the formation of the rhomboidal platelets and decreases the formation of rosette agglomerations as the concentration of the copolymer increases. For the material prepared without PAAMA the crystals have rough and ill-defined edges leading to hexagonal particles. When PAAMA is added (P-VPO5 and P-VPD15) the hexagonal crystallites become more regular, with well defined edges. When the concentration of PAAMA is increased (P-VPO15 and P-VPD25) only well defined edges of rhomboidal and hexagonal platelet morphologies are observed, without any presence of rosette agglomerates. Furthermore, the addition of PAAMA increases the relative intensity of the (001) reflection compared to the (220) reflection, as the concentration of the copolymer increases. Table 1 summarises the effect of PAAMA concentration on the surface area and morphology of P-VPO and P-VPD precursors.

In our previous study[26] PSMA could only be used to synthesise catalysts *via* the VPO route as it was found to be insoluble when added into the reduction step of $VOPO_4 \cdot 2H_2O$. In this study, the higher solubility of PAAMA allowed us to investigate this methodology for catalysts synthesized *via* the VPD route as well as the VPO route. Furthermore, higher concentrations of PAAMA could be added, leading to a thin platelet morphology with a high (001)/(220) reflection ratio.

3.2. *n*-Butane oxidation studies and post-reaction characterisation

All precursor materials were activated *in situ* and tested as catalysts for butane oxidation. The performance of a standard catalyst (P-VPO0) (Fig. 3a) gradually increases as the $VOHPO_4 \cdot 0.5H_2O$ precursor is gradually transformed to the active catalyst ($(VO)_2P_2O_7$ with some V^{5+} phases) over a period of several days before it equilibrates and reaches a steady state performance.[28] P-VPO5, the precursor that contains characteristic rosette-like agglomerates with isolated rhomboidal platelets, was found to activate over a shorter period of time compared to the standard vanadium phosphate materials with a comparable performance (Fig. 3b). The precursors (P-VPO15 and P-VPO25) also reached steady-state performance quickly (<10 h), but were found to be less active and selective to maleic anhydride compared to the P-VPO0 and P-VPO5 precursors (Fig. 3c and d). Table 2 shows the normalised rates after 20 h of the reaction and at steady state for each catalyst. The variation in catalyst

Table 1 The effect of PAAMA concentration on the morphology of P-VPO and P-VPD precursors and the relative intensity of the (001)/(220) reflections from XRD

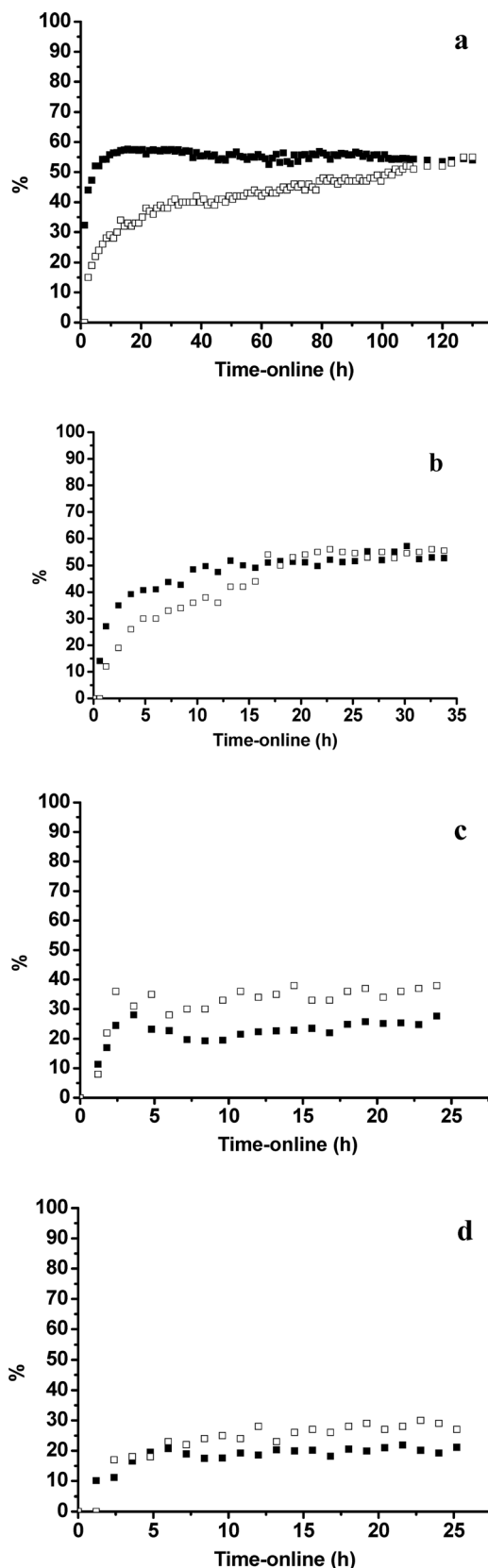| Concentration of PAAMA (g L^{-1})	P-VPO precursor			P-VPD precursor		
	Relative intensity (001)/(220)	Catalyst surface area (m^2 g^{-1})	Morphology	Relative intensity (001)/(220)	Catalyst surface area (m^2 g^{-1})	Morphology
0	0.35	11	Rosette-like	0.42	13	Rosette-like
5	1.40	12	Characteristic rosette-like agglomerates with isolated rhomboidal platelets	1.08	13	Characteristic rosette-like agglomerates
15	5.14	11	Isolated rhomboidal platelets	1.35	15	Characteristic rosette-like agglomerates with isolated rhomboidal platelets
25	5.20	10	Isolated rhomboidal and irregular platelets	1.77	13	Isolated rhomboidal platelets

Table 2 The normalised rates of VPO catalysts

Catalyst	Rate after 20 h (mole MA m^{-2} h^{-1})	Rate at steady state (mole MA m^{-2} h^{-1})
CVPO0	1.7×10^{-5}	2.4×10^{-5}
CVPO5	2.2×10^{-5}	2.3×10^{-5}
CVPO15	0.8×10^{-5}	0.9×10^{-5}
CVPO25	0.4×10^{-5}	0.4×10^{-5}

performance can be understood from the post reaction characterization of the catalysts. The XRD patterns of the activated catalysts C-VPO0 and C-VPO5 (Fig. 4a) illustrate that the precursor transformed from $VOHPO_4 \cdot 0.5H_2O$ to $(VO)_2P_2O_7$; which is widely considered to be the active/selective phase for butane oxidation. This transformation has been shown to be topotactic, with the (001) plane of the $VOHPO_4 \cdot 0.5H_2O$ precursor equivalent to the (200) plane in $(VO)_2P_2O_7$.[16,29,30] Therefore, the high (001)/(220) ratio of P-VPO5 compared with P-VPO0 leads to a $(VO)_2P_2O_7$ XRD pattern with a more intense (200) reflection in C-VPO5 compared to the standard material. This indicates that the morphology of the precursor is retained and the final catalyst and contains thinner platelets of $(VO)_2P_2O_7$ for the materials prepared using the copolymer structure directing agent than for the standard material. The fast activation observed for P-VPO5 can be attributed to the thinner platelets as this facilitates the removal of water from the $VOHPO_4 \cdot 0.5H_2O$ lattice during the activation. The precursors P-VPO15 and P-VPO25, which exhibited low catalytic activity, were found to contain a mixture of $(VO)_2P_2O_7$ and α_{II}-$VOPO_4$ phases (Fig. 4a), which was confirmed by Raman spectroscopy (Fig. 4b) that clearly shows that the very thin plate morphology that is achieved with high levels of PAAMA in the synthesis are more prone to oxidation during the activation. In these samples a shoulder appears on the $(VO)_2P_2O_7$ (200) reflection which could be indicative of the X1 phase,[3] which has recently been shown by DFT to provide a low energy pathway for butane to maleic anhydride.[31,32]

SEM micrographs for the post reaction catalysts C-VPO0, C-VPO5, C-VPO15 and C-VPO25 (Fig. 4c) show the same morphology observed in precursor materials P-VPO0, P-VPO5, P-VPO15 and P-VPO25 (Fig. 1b), confirming the previous findings that this reaction is topotactic.[16,29,30] We demonstrated from our previous TEM studies of catalysts prepared with PSMA[26] that, although the interior of the platelets are crystalline, an amorphous rim forms around the edge of the platelet. This is in keeping with our previous observations that the active site for butane oxidation is an amorphous overlayer on a crystalline or an amorphous bulk support.[33–35]

The precursors that we were able to synthesise *via* the VPD route using PAAMA were found to show similar behaviour to those prepared using the VPO route. P-VPD0 and P-VPD5, that have a rosette morphology, were activated over several days as the $VOHPO_4 \cdot 0.5H_2O$ precursor was gradually transformed *in situ* to the active catalyst $((VO)_2P_2O_7$ with some V^{5+} phases) (Fig. 5a and b respectively). P-VPD15, which
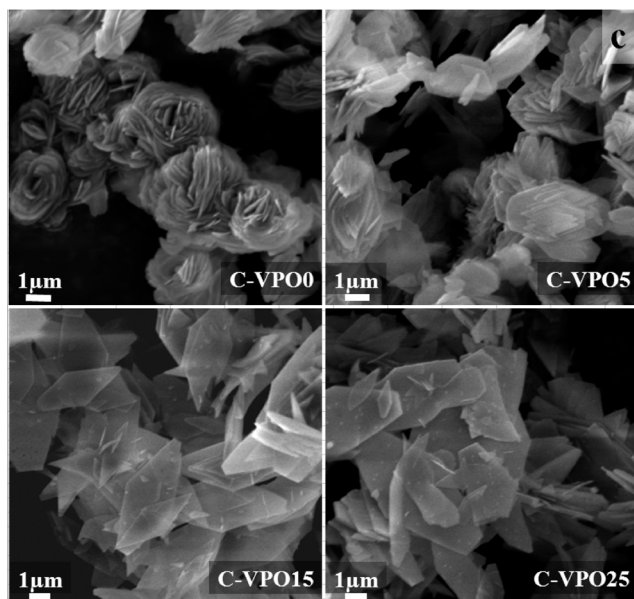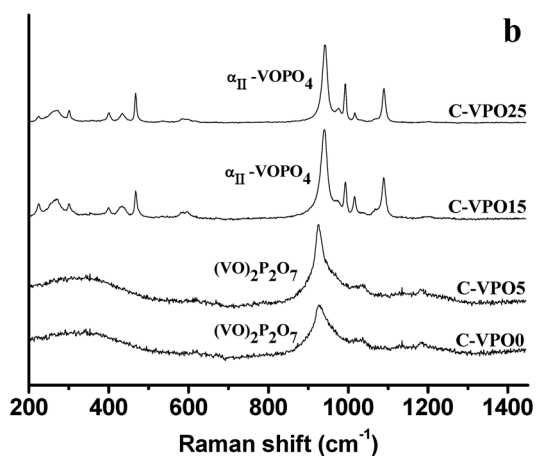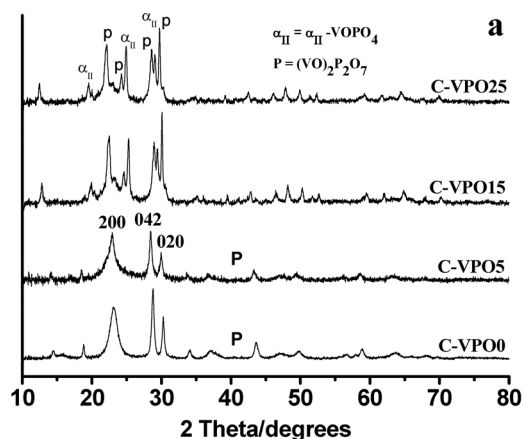
Fig. 3 Butane oxidation over: (a) P-VPO0 – steady state performance is reached after >100 h on line; (b) P-VPO5 – steady state performance is reached after <18 h on line; (c) P-VPO15 and (d) P-VPO25 – dramatic decrease in conversion and selectivity. (■) Conversion; (□) maleic anhydride selectivity. 1.7% butane in air, 400 °C, 3000 h^{-1} GHSV.

Fig. 4 (a) Powder XRD patterns, (b) Raman spectra and (c) SEM micrographs of C–VPO catalysts.

Fig. 5 Butane oxidation over: (a) P-VPD0 – steady state performance is reached after >100 h on line; (b) P-VPD5 – steady state performance is reached after >100 h on line; (c) P-VPD15 – steady state performance is reached after >15 and (d) P-VPD25 – dramatic decrease in conversion and selectivity. (■) Conversion; (□) maleic anhydride selectivity. 1.7% butane in air, 400 °C, 3000 h^{-1} GHSV.

contains characteristic rosette-like agglomerates with isolated rhomboidal platelets, activated in a shorter time compared to P-VPD0 (Fig. 5c) and achieved a comparable steady state
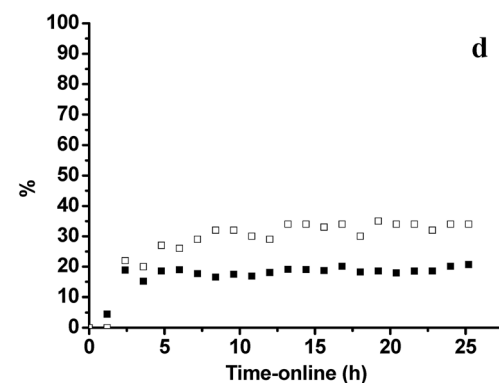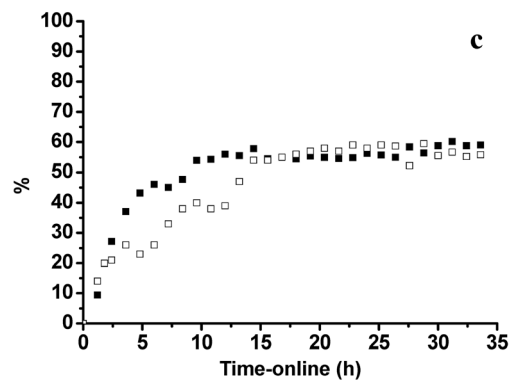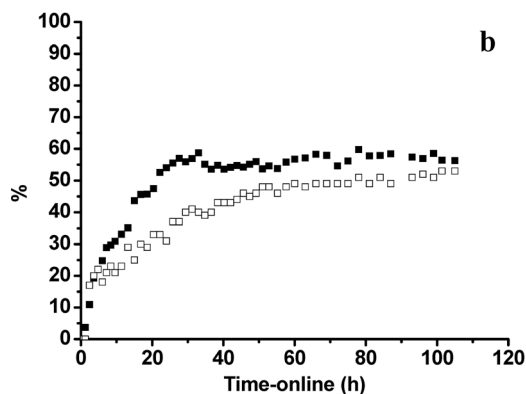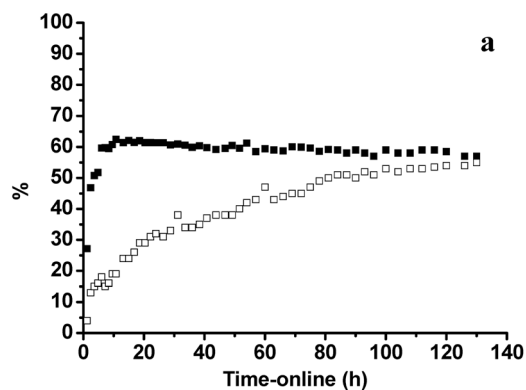
Table 3 The normalised rates of VPD catalysts

Catalyst	Rate after 20 h (mole MA m^{-2} h^{-1})	Rate at steady state (mole MA m^{-2} h^{-1})
CVPD0	1.3×10^{-5}	2.2×10^{-5}
CVPD5	1.2×10^{-5}	2.1×10^{-5}
CVPD15	1.9×10^{-5}	2.1×10^{-5}
CVPD25	0.5×10^{-5}	0.5×10^{-5}

performance after just 15 h on-line. Table 3 shows the normalised rates after 20 h of the reaction and at steady state for each catalyst. It is clear from this that C-VPD0, C-VPD5 and C-VPD15 all end up with similar performance, but that C-VPD15 reaches this level much faster than the other catalysts.

SEM confirmed that a topotactic transformation had taken place, and the morphology of the precursors is retained in the active catalysts (Fig. 6a). The XRD patterns for the activated catalysts (Fig. 6b) show that the C-VPD15 catalyst has a sharper and more intense (200) reflection of $(VO)_2P_2O_7$ compared to those of catalysts C-VPD0 and C-VPD5; which illustrates the thinner platelet morphology which leads to the fast activation of the precursor. A dramatic drop in conversion and selectivity was observed for C-VPD25 (Fig. 5d) and this was found to contain large amounts of α_{II}-VOPO$_4$ by XRD and Raman spectroscopy (Fig. 6b and c), confirming the findings for the VPO catalysts, that a very thin platelet morphology leads to oxidised catalysts.

In this study we found that only the characteristic rosette-like agglomerates with an isolated rhomboidal platelet morphology and a relative intensity ratio of *ca.* 1.4 for the (001)/(220) reflections are activated in a very short time (P-VPO5 and P-VPD15), and show good performance as catalysts for the selective oxidation of butane to maleic anhydride. It seems that an optimum concentration of the copolymer is needed to form a precursor with these features. However, the thin platelet morphology which is formed by the addition of high concentrations of PAAMA, and is characterised by a high relative intensity of the (001) reflection, exhibit poor catalytic performance as the thin plates are easily oxidised to VOPO$_4$.

4. Conclusions

Using PAAMA in the preparation of vanadium phosphate catalysts has been shown to influence the morphology of the resultant precursors as well as performance of their corresponding catalysts. It has been found that the addition of PAAMA increased the crystallinity of the synthesised precursors and as the concentration of PAAMA increased the morphology changed from rosette-like clusters; to rosette-like agglomerates with isolated rhomboidal platelets; and eventually to isolated platelets. The XRD patterns showed that with the addition of PAAMA the relative intensity ratio of the
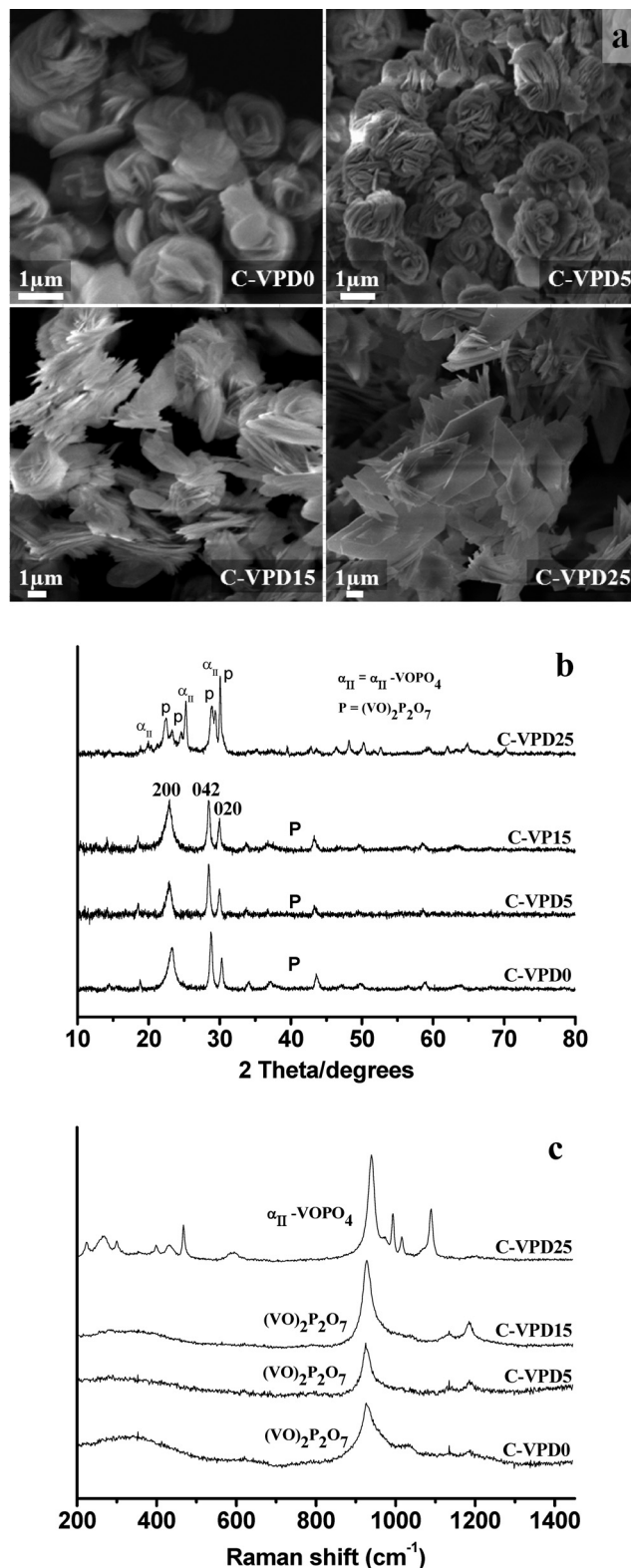

Fig. 6 (a) SEM micrographs, (b) powder XRD Patterns, and (c) Raman spectra of C-VPD catalysts.

(001)/(220) reflections were found to increase during this change in morphology. This could be ascribed to the copolymer acting as a structure directing agent that can interact

with the (001) plane of $VOHPO_4 \cdot 0.5H_2O$, preventing growth in this direction leading to thinner platelets.

When these materials were investigated as catalysts for butane oxidation they exhibited different activation behaviours. The precursors synthesised using PAAMA which had a relative intensity ratio of the (001)/(220) reflections of around 1.4 activated much faster *in situ* to the active catalyst compared to the precursors prepared using the standard methodology. However, precursors with a morphology comprising of isolated platelets and a high relative intensity of the (001) reflection displayed poor performance as they were oxidised to α_{II}-$VOPO_4$ phases during activation. An optimum concentration of PAAMA is required to control the features of the synthesised precursor to achieve an active catalyst.

Acknowledgements

References

1 J. K. Bartley, I. J. Ellison, A. Delimitis, C. J. Kiely, A. Z. Isfahani, C. Rhodes and G. J. Hutchings, *Phys. Chem. Chem. Phys.*, 2001, **3**, 4606.

2 J. A. Lopez-Sanchez, J. K. Bartley, R. P. K. Wells, C. Rhodes and G. J. Hutchings, *New J. Chem.*, 2002, **26**, 1613.

3 T. Shimoda, T. Okuhara and M. Misono, *Bull. Chem. Soc. Jpn.*, 1985, **58**, 2163.

4 G. Poli, I. Resta, O. Ruggeri and F. Trifirò, *Appl. Catal.*, 1981, **1**, 395.

5 N. Mizuno, H. Hatayama and M. Misono, *Chem. Mater.*, 1997, **9**, 2697.

6 M. O'Connor, F. Dason and B. K. Hodnett, *Appl. Catal.*, 1990, **64**, 161.

7 F. Cavani, G. Centi and F. Trifirò, *Appl. Catal.*, 1984, **4**, 191.

8 L. Griesel, J. K. Bartley, R. P. K. Wells and G. J. Hutchings, *J. Mol. Catal.*, 2004, **220**, 113.

9 J. K. Bartley, J. A. Lopez-Sanchez and G. J. Hutchings, *Catal. Today*, 2003, **81**, 197.

10 T. Doi and T. Miyake, *Appl. Catal., A*, 1997, **164**, 141.

11 T. Miyake and T. Doi, *Appl. Catal.*, 1995, **131**, 43.

12 N. Guilhaume, M. Roullet, G. Pajonk, B. Grzybowska and J. C. Volta, *Stud. Surf. Sci. Catal.*, 1992, **72**, 255.

13 J. K. Bartley, R. P. K. Wells and G. J. Hutchings, *J. Catal.*, 2000, **195**, 423.

14 J. K. Bartley, R. P. K. Wells and G. J. Hutchings, *Catal. Lett.*, 2001, **72**, 99.

15 I. J. Ellison, G. J. Hutchings, M. T. Sananés and J. C. Volta, *J. Chem. Soc., Chem. Commun.*, 1994, 1093.

16 J. W. Johnson, D. C. Johnston, A. J. Jacobson and J. F. Brody, *J. Am. Chem. Soc.*, 1984, **106**, 8123.

17 H. S. Horowitz, C. M. Blackstone, A. W. Sleight and G. Teufer, *Appl. Catal.*, 1988, **38**, 193.

18 G. J. Hutchings, M. T. Sananés, S. Sajip, C. J. Kiely, A. Burrows, I. J. Ellison and J. C. Volta, *Catal. Today*, 1997, **33**, 161.

19 S. Mann, *Nature*, 1993, **365**, 499.

20 L. M. Qi, J. Li and J. M. Ma, *Adv. Mater.*, 2002, **14**, 300.

21 L. M. Qi, H. Colfen and M. Antonietti, *Chem. Mater.*, 2000, **12**, 2392.

22 X. Zhao, J. Yu and B. Cheng, *Mater. Chem. Phys.*, 2007, **101**, 379.

23 J. Yu, H. Tang, B. Cheng and X. Zhao, *J. Solid State Chem.*, 2004, **177**, 3368.

24 D. D. L. Chung, *J. Mater. Sci.*, 2004, **39**, 2973.

25 N. P. Singh and N. B. Singh, *Prog. Cryst. Growth Charact. Mater.*, 2006, **52**, 84.

26 Z. Lin, W. Weng, C. J. Kiely, N. F. Dummer, J. K. Bartley and G. J. Hutchings, *Catal. Today*, 2010, **157**, 211.

27 G. J. Hutchings, C. J. Kiely, M. T. Sananes-Schulz, A. Burrows and J. C. Volta, *Catal. Today*, 1998, **40**, 273.

28 E. A. Lombardo, C. A. Sánchez and L. M. Cornaglia, *Catal. Today*, 1992, **15**, 407.

29 P. T. Nguyen, A. W. Sleight, N. Roberts and W. W. Warren, *J. Solid State Chem.*, 1996, **122**, 259.

30 C. J. Kiely, A. Burrows, G. J. Hutchings, K. E. Béré, J. C. Volta, A. Tuel and M. Abon, *Faraday Discuss.*, 1996, **105**, 103.

31 M. J. Cheng, W. A. Goddard and R. Fu, *Top. Catal.*, 2014, **57**, 1171.

32 M. J. Cheng and W. A. Goddard, *J. Am. Chem. Soc.*, 2013, **135**, 4600.

33 G. J. Hutchings, A. Desmartin-Chomel, R. Olier and J. C. Volta, *Nature*, 1994, **368**, 41.

34 C. J. Kiely, A. Burrows, S. Sajip, G. J. Hutchings, M. T. Sananés, A. Tuel and J. C. Volta, *J. Catal.*, 1996, **162**, 31.

35 S. Sajip, C. Rhodes, J. K. Bartley, A. Burrows, C. J. Kiely and G. J. Hutchings, in *Catalytic Activation and Functionalisation of Light Alkanes*, ed. E. G. Derouane, J. Haber, F. Lemos, F. Ramôa Ribeiro and M. Guisnet, Kluwer Academic Publishers, 1998, pp. 429–433.